UNIVERSITY OF CALIFORNIA SAN DIEGO

Adaptive Control of an Aircraft in Icing Using a Batch Least-Squares Identifier

A thesis submitted in partial satisfaction
of the requirements for the degree of
Master of Science

in

Engineering Sciences (Aerospace Engineering)

by

Samer Shaghoury

Committee in charge:

Professor Miroslav Krstić, Chair
Professor Jorge Cortes
Professor Raymond de Callafon

2020

The Thesis of Samer Shaghoury is approved, and it is acceptable in quality and form for publication on microfilm and electronically:

Chair

University of California

2020

Dedication

To my caring wife,

The love we will share,

The family we will build,

And the Light we will shine.

Table of Contents

List of Abbreviations

A	Aircraft
AC	Aerodynamic Center
AIAA	American Institute of Aeronautics and Astronautics
AOA	Angle of Attack
B, BAS	Body Axis System
BaLSI	Batch Least-Squares Identifier
CEC	Certainty-Equivalence Controller
CG	Center of Gravity
D	Drag
E, EAS	Earth Axis System
Est.	Estimation
FAA	Federal Aviation Administration
H, HT	Horizontal Tail
ISS	Input-to-State Stable
L	Lift
NASA	National Aeronautics and Space Administration
ODE	Ordinary Differential Equations
Par.	Parameter
USAF	United States Air Force
W	Wing
e	Elevator
f	Flap
m	Pitching Moment
s	Stall

List of Symbols

Δ control-surface deflection impact to AOA

H set of possible internal-dynamics state vectors

Φ set of possible unknown-parameter vectors

α AOA

β tunable BaLSI parameter

γ BaLSI ODE variable

γ flight-path angle

δ control-surface deflection

ϵ tunable BaLSI parameter

η downwash factor

η internal-dynamics state

θ pitch angle

λ icing factor for drag

ρ air density

σ icing factor for lift

ϕ thrust-vector angle

ϕ unknown-parameter vector

B BaLSI ODE variable

C aerodynamic coefficient

$\bar{C}$ BaLSI selection matrix

D drag

F force

I moment of inertia

L lift

$\mathcal{L}$ Lie derivative

M moment

Q BaLSI ODE variable

$\mathbb{R}$ the set of real numbers

S planform area

T thrust

T tunable BaLSI parameter

$\mathcal{U}$ set of possible inputs

V Lyapunov function

$\mathcal{X}$ set of possible state vectors

Y BaLSI ODE variable

$\mathbb{Z}$ the set of integers

$a(\cdot)$ tunable BaLSI parameter

c controller gain

$\bar{c}$ mean chord

$f(\cdot)$ system mapping

g gravity

$g(\cdot)$ system mapping

$h(\cdot)$	output function
k	lift-induced-drag factor
l	number of unknown parameters
m	mass
m	number of inputs
n	number of states
$\bar{q}$	dynamic pressure
t	time
u	input
v	airspeed
w	BaLSI ODE variable
x	position along the x axis
x	state vector
y	position along the y axis
y	output
z	position along the z axis
z	BaLSI ODE variable

List of Figures

Acknowledgements

I would like to thank my advisor and committee chair, Professor Miroslav Krstić. I am especially grateful for his guidance, advice, and support, as his technical expertise and experience has proven invaluable. I would also like to thank my committee members, Professors Raymond de Callafon and Jorge Cortes, for their time, attentiveness, and feedback.

This thesis, in part, is currently being prepared for submission for publication of the material. Shaghoury, Samer; Krstić, Miroslav. The thesis author was the primary investigator and author of this material.

Abstract of the Thesis

Adaptive Control of an Aircraft in Icing Using a Batch Least-Squares Identifier

by

Samer Shaghoury

Master of Science in Engineering Science (Aerospace Engineering)

University of California San Diego, 2020

Professor Miroslav Krstić, Chair

Extensive effort in controller design of aircraft systems is invested in robustness to ensure safe, stable behavior. Particular attention is placed on anomalous flight-conditions harbored by the atmosphere, especially icing. The thesis presents a regulation trigger-based adaptive controller to cope mathematically with the impact of ice on the aircraft equations of motion and control the aircraft pitch to the commanded angle. Upon an introduction to the problem, a pitch model of an aircraft system is

derived, where the impact of icing is modeled. The design of a stabilizing certainty-equivalence controller utilizing backstepping follows, and is succeeded by the introduction of the Batch Least-Squares Identifier (BaLSI). Finally, simulation results of an aircraft experiencing icing demonstrates the effectiveness of the identifier, with the trajectory of the iced system utilizing the proposed identifier closely following that of the nominal system.

Chapter 1

Introduction

1.1 Background

Aircraft generally avoid flying in known icing conditions at all costs, but inadvertent icing events frequently occur. Although many aircraft utilize ice detectors, few employ ice-shedding mechanisms. Upon detection of icing conditions, pilots must maneuver out of the conditions, during which, ice may continuously encroach upon the aircraft. Icing causes a variety of issues, including degraded engine and aerodynamic performance, the latter of which is the focus of the thesis.

Ice accretion can be pernicious in nature and, therefore, difficult to estimate the severity of by a pilot. Although impacts to lift and drag may be discerned, stability, especially in unmanned systems, may be lost suddenly. Significant attention in test and research have focused on controlling ice-related risk by improving methods in ice forecasting and detection, ice sublimation, and flight controls.

1.2 History of Aircraft Icing

Motivation for mitigating icing risks in aircraft has existed for a majority of aircraft history. Over time, demand for all-weather capability (especially in military

aircraft) and ice-related mishaps, among other reasons, have contributed to an increase in resources devoted to solving the icing dilemma. In the name of mishap prevention, the Federal Aviation Administration (FAA) began requiring certifications for flight in icing, further increasing the demand.

Substantial effort in the development of detection and sublimation technologies, along with methodologies for modeling ice accretion and evaluating performance, stability, and control degradation, was made under the auspices of the National Aeronautics and Space Administration (NASA). [1] details NASA's history of contributions up to 1989. In 1991, the FAA's attention on the matter culminated into the publishing of [2], a three-volume handbook dedicated solely to in-flight icing. The FAA maintains guides and references for flight in adverse weather and icing in [3] and [4]. [5] details industry's progress in icing-related work in 2000, presenting the physics behind ice accretion and the latest methods in ice modeling and simulation.

Even with the progress in the 20th century, application of the technologies and methodologies developed were limited as detailed in [6], which also presents a simpler modeling approach. With late-century advancements to computing accelerating improvements to ice-accretion modeling and simulation, advancements in the understanding of ice's impacts to aircraft, which seldom went beyond two-dimensions, remained unripe for use in control-law development. Research typically followed suit of [7] to increase understanding of ice's impacts on aircraft performance, stability, and control by use of aircraft models in wind tunnels; however, the results remained limited to specific aircraft configurations and ice formations.

Attempts to remedy the specific nature of results plaguing ice-impact studies gained traction with the exploitation of system identification and adaptive control. [8] incorporated system identification in flight-envelope estimation, which was successfully applied to an icing scenario. [9] utilized system identification for evaluation of an icing-severity factor. $\mathcal{L}_1$ adaptive control is among adaptive-control methods to have entered flight-control applications, presented in [10] in 2010 and again in [11] in 2012. In 2014, [12] employed adaptive control for the task of output tracking, applying the methodology to an aircraft with failed actuators.

Only recently have adaptive control methods been applied to aircraft in icing in research. In 2014, [13] utilized an adaptive output tracking scheme to attempt to control a linearized, iced aircraft model. The proposed scheme, however, was unable to ensure full control of all aircraft axes and guarantee convergence of parameter estimates (used to model ice's impacts). In 2015, [14] utilized predictive control in conjunction with an extended Kalman filter to successfully control a simulated Airbus aircraft; however, the scheme requires system excitation and did not produce estimates of icing impacts.

1.3 Batch Least-Squares Identifier

The thesis will apply the Batch Least-Squares Identifier (BaLSI) [15]—an event-triggered, parameter update law to estimate unknown icing parameters in an aircraft model via least-squares methodology. The proposed adaptive-control scheme will utilize a Certainty-Equivalence Controller (CEC) in conjunction with the BaLSI to stabilize an aircraft model. The BaLSI's approach presents multiple advantages, namely

the guarantees of convergence of parameter estimations and asymptotic stability of the system (subject to assumptions). The adaptive-control scheme was shown to achieve asymptotic stability of a wing-rock model in the presence of five (5) uncertainties in [15] and a two-link robot in the presence of four (4) uncertainties in [16].

1.4 Thesis Outline

Beyond the introduction, the thesis is organized as follows. In Chapter 2, the pitch model of an aircraft is derived, followed by the modeling of ice's impacts and plant construction. A stabilizing CEC is derived in Chapter 3, and the BaLSI extension to the controller is presented in Chapter 4. Simulation results of the iced system is presented in Chapter 5. Conclusions and recommendations are given in Chapter 6, followed by the bibliography in Chapter 7.

Chapter 2

Derivation of the Aircraft Model

2.1 Coordinate System

Two coordinate systems are utilized: the Earth Axis System (EAS) and the Body Axis System (BAS). The model will only concern longitudinal motion, thus allowing for the following assumption to make defining the EAS more convenient.

Assumption 2.1 The aircraft experiences no lateral-directional movement.

Typically, the EAS x axis is pointing North and y East; however, Assumption 2.1 allows for the following definition:

- x_E axis is within the horizontal plane in the direction of the aircraft heading, positive fore.
- y_E axis is within the horizontal plane orthogonal to the x_E axis, positive to the right.
- z_E axis is orthogonal to the x_E and y_E axes, positive downwards.

The BAS is defined as follows:

- x_B (longitudinal) axis is along the fuselage centerline, positive fore.
- y_B (lateral) axis is along the wing span, orthogonal to the x_B axis, positive out the right wing.
- z_B (directional) axis is orthogonal to the x_B and y_B axes, positive through the bottom of the aircraft.

Pitch refers to movement about the lateral axis and is positive counterclockwise (nose up). The pitch angle refers to the angle between the x_B axis and the x_E-y_E plane. The Angle of Attack (AOA) is the angle between the x_B axis and the relative wind. The flight-path angle is the angle between the relative wind and the x_E-y_E plane. The relationship between pitch, AOA, and flight-path angle (θ, α, and γ, respectively) is

$$\theta = \alpha + \gamma \tag{2-1}$$

The flight-path angle can be calculated as

$$\gamma = \text{atan}\left(-\frac{\dot{z}_E}{\dot{x}_E}\right) \tag{2-2}$$

2.2 Equations of Motion

2.2.1 Preliminary Assumptions

To derive the model, a standard aircraft configuration is assumed, as described in Assumption 2.2.

Assumption 2.2 The aircraft is of a standard configuration (i.e., utilizing a non-lifting fuselage, a wing, and a horizontal tail aft of the wing).

Assumption 2.3 below is used to keep airspeed constant. Enough negative pitch can result in negative thrust; therefore, the model will be restricted by Assumption 2.4.

Assumption 2.3 Thrust will always be such that airspeed is constant.

Assumption 2.4 The aircraft pitch is greater than or equal to zero.

The assumptions are not too restrictive, as Assumption 2.3 is generally a primary goal of thrust, and aircraft (especially larger aircraft) frequently climb to exit icing conditions [3]. A third assumption regarding thrust will be made, setting the thrust-vector angle, ϕ, to 0.

Assumption 2.5 Thrust is only applied in the longitudinal direction.

The next assumption allows easy modeling of aerodynamic lift and drag.

Assumption 2.6 Lift is linearly proportional to the AOA, and drag quadratically (symmetric with respect to zero AOA).

Assumption 2.6 is generally accurate up to near-stall conditions; therefore, the model will limit the AOA. To further simplify the model, the following assumption is also made.

Assumption 2.7 Thrust and drag contributions to pitching moment are negligible.

2.2.2 Aerodynamic Forces and Moments

Lift, L, produced by the wing and Horizontal Tail (HT) are modeled as

$$L_W = \bar{q}(SC_L)_W = \bar{q}S_W\left(C_{L_{0_W}} + C_{L_{\alpha_W}}(\alpha + \Delta_f\delta_f)\right) \tag{2-3}$$

$$L_H = \bar{q}(SC_L)_H = \bar{q}S_H\left(C_{L_{0_H}} + C_{L_{\alpha_H}}(\alpha + \Delta_e\delta_e)\right) \tag{2-4}$$

$\bar{q}$ is the dynamic pressure, S is the planform area, C_{L_0} is the lift coefficient (C_L) at $\alpha = 0$, C_{L_α} is the C_L-α slope, and Δ is the α-δ slope (deflections, δ, positive trailing-edge down). Flap deflection is taken as constant. Wing downwash is modeled by applying constants to the dynamic pressure and AOA seen by the HT (η_q and η_α, respectively). (2-4) is rewritten as

$$L_H = \eta_q\bar{q}S_H\left(C_{L_{0_H}} + C_{L_{\alpha_H}}\eta_\alpha(\alpha + \Delta_e\delta_e)\right) \tag{2-5}$$

The total aircraft lift is

$$L = L_W + L_H = \bar{q}\left(L_0 + L_\alpha\alpha + L_{\delta_e}\delta_e\right) \tag{2-6}$$

where

$$\begin{gathered} L_0 = L_{0_W} + L_{0_H} \\ L_\alpha = L_{\alpha_W} + L_{\alpha_H} \qquad L_{\delta_e} = \eta_q \eta_\alpha S_H C_{L_{\alpha_H}} \Delta_e \\ L_{0_W} = S_W \left(C_{L_{0_W}} + C_{L_{\alpha_W}} \Delta_f \delta_f \right) \qquad L_{0_H} = \eta_q S_H C_{L_{0_H}} \\ L_{\alpha_W} = S_W C_{L_{\alpha_W}} \qquad L_{\alpha_H} = \eta_q \eta_\alpha S_H C_{L_{\alpha_H}} \end{gathered} \tag{2-7}$$

The drag produced by the wing, HT, and aircraft are

$$D_W = \bar{q}(SC_D)_W = \bar{q} S_W \left(C_{D_{0_W}} + k_W \left(\alpha + \Delta_f \delta_f \right)^2 \right) \tag{2-8}$$

$$D_H = \bar{q}(SC_D)_H = \eta_q \bar{q} S_H \left(C_{D_{0_H}} + k_H \eta_\alpha^2 (\alpha + \Delta_e \delta_e)^2 \right) \tag{2-9}$$

$$D_A = \bar{q} S_W C_{D_A} \tag{2-10}$$

C_{D_0} is the drag coefficient (C_D) at $C_L = 0$, and k is the drag-due-to-lift factor. The aircraft drag coefficient, C_{D_A}, is taken to be constant. The total aircraft drag is

$$D = D_A + D_W + D_H = \bar{q} \left(D_0 + k_1 \left(\alpha + \Delta_f \delta_f \right)^2 + k_2 (\alpha + \Delta_e \delta_e)^2 \right) \tag{2-11}$$

where

$$\begin{gathered} D_0 = D_{0_A} + D_{0_W} + D_{0_H} \\ k_1 = S_W k_W \qquad k_2 = \eta_q \eta_\alpha^2 S_H k_H \\ D_{0_A} = S_W C_{D_A} \qquad D_{0_W} = S_W C_{D_{0_W}} \qquad D_{0_H} = \eta_q S_H C_{D_{0_H}} \end{gathered} \tag{2-12}$$

Pitching-moments about the Aerodynamic Center (AC) are separated into three components: wing, HT, and all other contributions. The latter is modeled as

$$M_A = \bar{q} C_{m_A} (S\bar{c})_W = \bar{q} S_W \bar{c}_W \left(C_{m_{0_A}} + C_{m_{\alpha_A}} \alpha \right) \tag{2-13}$$

$\bar{c}$ is the mean chord, C_{m_0} is the pitching moment (C_m) at $\alpha = 0$ and C_{m_α} is the C_m-α slope. The wing and HT contributions are

$$M_W = L_W \cos\alpha \left(x_{W_{AC}} - x_{CG} \right) = L_W \bar{x}_W \cos\alpha \tag{2-14}$$

$$M_H = L_H \cos\alpha \left(x_{H_{AC}} - x_{CG} \right) = L_H \bar{x}_H \cos\alpha \tag{2-15}$$

2.2.3 Force Model

Force models are derived using Newton's 2nd law, applied in the EAS:

$$m\ddot{x}_E = \left(\sum F_x \right)_E = -L \sin\gamma - D \cos\gamma + T \cos(\theta + \phi) \tag{2-16}$$

$$m\ddot{z}_E = \left(\sum F_z \right)_E = mg - L \cos\gamma + D \sin\gamma - T \sin(\theta + \phi) \tag{2-17}$$

Note that per Assumption 2.5, $\phi = 0$. Substituting in (2-6) and (2-11):

$$m\ddot{x}_E = -\bar{q}\Big[\big(L_0 + L_\alpha\alpha + L_{\delta_e}\delta_e\big)\sin\gamma + \Big(D_0 + k_1\big(\alpha + \Delta_f\delta_f\big)^2 + k_2(\alpha + \Delta_e\delta_e)^2\Big)\cos\gamma\Big] + T\cos\theta \tag{2-18}$$

$$m\ddot{z}_E = mg + \bar{q}\Big[-\big(L_0 + L_\alpha\alpha + L_{\delta_e}\delta_e\big)\cos\gamma + \Big(D_0 + k_1\big(\alpha + \Delta_f\delta_f\big)^2 + k_2(\alpha + \Delta_e\delta_e)^2\Big)\sin\gamma\Big] - T\sin\theta \tag{2-19}$$

Per Assumption 2.3, the airspeed will be kept constant, meaning acceleration must equal zero. The expression for acceleration is derived:

$$\dot{v} = \frac{d}{dt}\sqrt{\dot{x}_E^2 + \dot{z}_E^2} = \frac{\dot{x}_E\ddot{x}_E + \dot{z}_E\ddot{z}_E}{\sqrt{\dot{x}_E^2 + \dot{z}_E^2}} = \ddot{x}_E\cos\gamma - \ddot{z}_E\sin\gamma \tag{2-20}$$

To keep $\dot{v} = 0$, the thrust at any point in time must be

$$T = \sec\alpha\left[\bar{q}\left(D_0 + k_1\big(\alpha + \Delta_f\delta_f\big)^2 + k_2(\alpha + \Delta_e\delta_e)^2\right) + mg\sin\gamma\right] \tag{2-21}$$

Given (2-21) and noting

$$\cos\gamma - \frac{\cos\theta}{\cos\alpha} \equiv \sin\gamma\tan\alpha \qquad 1 - \frac{\sin\theta\sin\gamma}{\cos\alpha} \equiv \frac{\cos\theta\cos\gamma}{\cos\alpha}$$
$$\sin\gamma - \frac{\sin\theta}{\cos\alpha} \equiv -\cos\gamma\tan\alpha \tag{2-22}$$

(2-18) and (2-19) can be written as

$$m\ddot{x}_E = \left\{ mg\left(\frac{\cos\theta}{\cos\alpha}\right) - \bar{q}\left[\left(L_0 + L_\alpha\alpha + L_{\delta_e}\delta_e\right) + \left(D_0 + k_1\left(\alpha + \Delta_f\delta_f\right)^2 + k_2(\alpha + \Delta_e\delta_e)^2\right)\tan\alpha\right]\right\}\sin\gamma \tag{2-23}$$

$$m\ddot{z}_E = \left\{ mg\left(\frac{\cos\theta}{\cos\alpha}\right) - \bar{q}\left[\left(L_0 + L_\alpha\alpha + L_{\delta_e}\delta_e\right) + \left(D_0 + k_1\left(\alpha + \Delta_f\delta_f\right)^2 + k_2(\alpha + \Delta_e\delta_e)^2\right)\tan\alpha\right]\right\}\cos\gamma \tag{2-24}$$

2.2.4 Moment Model

The moment model will be based off

$$I_{yy}\ddot{\theta} = \sum M_{CG} = M_A + (L_W\bar{x}_W + L_H\bar{x}_H)\cos\alpha \tag{2-25}$$

Substituting the moment and lift equations into (2-25) yields

$$\ddot{\theta} = \bar{q}\{M_0 + \left(M_{c0_W} + M_{c0_H}\right)\cos\alpha + \left[M_\alpha + \left(M_{c\alpha_W} + M_{c\alpha_H}\right)\cos\alpha\right]\alpha + M_{\delta_e}\cos\alpha\,\delta_e\} \tag{2-26}$$

where

$$\begin{aligned} M_0 &= I_{yy}^{-1} S_W \bar{c}_W C_{m_{0_A}} \qquad M_\alpha = I_{yy}^{-1} S_W \bar{c}_W C_{m_{\alpha_A}} \\ M_{c0_W} &= I_{yy}^{-1} L_{0_W} \bar{x}_W \qquad M_{c0_H} = I_{yy}^{-1} L_{0_H} \bar{x}_H \\ M_{c\alpha_W} &= I_{yy}^{-1} L_{\alpha_W} \bar{x}_W \qquad M_{c\alpha_H} = I_{yy}^{-1} L_{\alpha_H} \bar{x}_H \\ M_{\delta_e} &= I_{yy}^{-1} L_{\delta_e} \bar{x}_H \end{aligned} \tag{2-27}$$

2.3 Modeling Impacts of Icing

Effects of icing on the equations presented thus far will now be assessed. The effects, which are of unknown magnitudes, will become the unknown parameters to be estimated by the BaLSI scheme. Icing generally first occurs on aerodynamic surfaces, resulting in decreased lift and increased drag; thus, impacts of icing will be modeled by multiplying the aerodynamic forces by icing factors per Assumption 2.8. Furthermore, the icing factors will be assumed constant per Assumption 2.9.

Assumption 2.8 Accumulated ice only impacts aerodynamics of the wing and HT.

Assumption 2.9 Icing factors are constant.

The decrease in lift and increase in drag will be modeled via the icing factors $0 < \sigma < 1$ and $\lambda > 1$, respectively. The icing factors will be applied to the wing and

HT aerodynamic forces. The impacts of the icing factors to the lift and moment constants defined in (2-7) and (2-12) are highlighted below:

$$\begin{gathered}
\left(L_{0_W}\right)_{ice} = \sigma_{0_W} S_W \left(C_{L_{0_W}} + C_{L_{\alpha_W}} \Delta_f \delta_f\right) \qquad \left(L_{0_H}\right)_{ice} = \sigma_{0_H} \eta_q S_H C_{L_{0_H}} \\
\left(L_{\alpha_W}\right)_{ice} = \sigma_{\alpha_W} S_W C_{L_{\alpha_W}} \qquad \left(L_{\alpha_H}\right)_{ice} = \sigma_{\alpha_H} \eta_q \eta_\alpha S_H C_{L_{\alpha_H}} \\
\left(L_{\delta_e}\right)_{ice} = \sigma_{\delta_H} \eta_q \eta_\alpha S_H C_{L_{\alpha_H}} \Delta_e
\end{gathered} \tag{2-28}$$

$$\begin{gathered}
\left(D_{0_W}\right)_{ice} = \lambda_{0_W} S_W C_{D_{0_W}} \qquad \left(D_{0_H}\right)_{ice} = \lambda_{0_H} \eta_q S_H C_{D_{0_H}} \\
(k_1)_{ice} = \lambda_{k_W} S_W k_W \qquad (k_2)_{ice} = \lambda_{k_H} \eta_q \eta_\alpha^2 S_H k_H
\end{gathered} \tag{2-29}$$

Note the constant D_{0_A}, representing the drag generated by the aircraft body, is not impacted by ice per Assumption 2.8. Furthermore, the moment constants defined in (2-27) are also impacted due to dependencies on the lift constants in (2-28).

The equations of motion in (2-23), (2-24), and (2-26) are now adapted for ice.

$$\begin{aligned}
m\ddot{x}_E = \Bigg\{ & mg\left(\frac{\cos\theta}{\cos\alpha}\right) \\
& - \bar{q}\Big[\left(\sigma_{0_W} L_{0_W} + \sigma_{0_H} L_{0_H} + \left(\sigma_{\alpha_W} L_{\alpha_W} + \sigma_{\alpha_H} L_{\alpha_H}\right)\alpha\right. \\
& \left. + \sigma_{\delta_H} L_{\delta_e} \delta_e\right) \\
& + \left(D_{0_A} + \lambda_{0_W} D_{0_W} + \lambda_{0_H} D_{0_H} + \lambda_{k_W} k_1 \left(\alpha + \Delta_f \delta_f\right)^2\right. \\
& \left. + \lambda_{k_H} k_2 (\alpha + \Delta_e \delta_e)^2\right) \tan\alpha\Big]\Bigg\} \sin\gamma
\end{aligned} \tag{2-30}$$

$$
\begin{aligned}
m\ddot{z}_E = \Big\{ & mg\left(\frac{\cos\theta}{\cos\alpha}\right) \\
& - \bar{q}\Big[\left(\sigma_{0_W} L_{0_W} + \sigma_{0_H} L_{0_H} + \left(\sigma_{\alpha_W} L_{\alpha_W} + \sigma_{\alpha_H} L_{\alpha_H}\right)\alpha\right. \\
& \left. + \sigma_{\delta_H} L_{\delta_e} \delta_e\right) \\
& + \Big(D_{0_A} + \lambda_{0_W} D_{0_W} + \lambda_{0_H} D_{0_H} + \lambda_{k_W} k_1 \left(\alpha + \Delta_f \delta_f\right)^2 \\
& + \lambda_{k_H} k_2 (\alpha + \Delta_e \delta_e)^2\Big) \tan\alpha\Big]\Big\} \cos\gamma
\end{aligned}
\tag{2-31}
$$

$$
\begin{aligned}
\ddot{\theta} = \bar{q}\{ & M_0 + \left(\sigma_{0_W} M_{c0_W} + \sigma_{0_H} M_{c0_H}\right)\cos\alpha \\
& + \left[M_\alpha + \left(\sigma_{\alpha_W} M_{c\alpha_W} + \sigma_{\alpha_H} M_{c\alpha_H}\right)\cos\alpha\right]\alpha \\
& + \sigma_{\delta_H} M_{\delta_e} \cos\alpha\, \delta_e\}
\end{aligned}
\tag{2-32}
$$

2.4 Plant Construction

Selection of the plant states will primarily be drawn from the desired variable to be controlled (pitch). An additional state, either γ or α, will be added so the system is not underdetermined. The state vector is defined as

$$
x = \begin{bmatrix} x_1 \\ x_2 \\ x_3 \end{bmatrix} = \begin{bmatrix} \theta - \bar{\theta} \\ \dot{\theta} \\ \alpha \end{bmatrix} \qquad x \in \mathcal{X} = \begin{bmatrix} [0° - \bar{\theta}, 180° - \bar{\theta}] \\ [\dot{\theta}_-, \dot{\theta}_+] \\ [\alpha_{s-}, \alpha_{s+}] \end{bmatrix} \subset \mathbb{R}^n \qquad n = 3 \tag{2-33}
$$

where the commanded pitch angle, $\bar{\theta} \in [0°, 180°]$, is constant. $\dot{\theta}_-$ and $\dot{\theta}_+$ are the pitch-rate limits, and α_{s-} and α_{s+} are the angles near stall at which lift can no longer be taken as linearly proportional AOA (per Assumption 2.6).

The input variable is defined as

$$u = \delta_e \qquad u \in \mathcal{U} = [\delta_{e-}, \delta_{e+}] \subset \mathbb{R}^m \qquad m = 1 \tag{2-34}$$

δ_{e-} and δ_{e+} are the elevator-deflection limits.

The time derivative of α will be obtained by taking the time derivative of (2-1):

$$\dot{\alpha} = \dot{\theta} - \dot{\gamma} \tag{2-35}$$

To obtain $\dot{\gamma}$, the time derivative of (2-2) is taken to obtain

$$\dot{\gamma} = \frac{d}{dt}\left[\operatorname{atan}\left(-\frac{\dot{z}_E}{\dot{x}_E}\right)\right] = -\frac{1}{v}(\ddot{z}_E \cos\gamma + \ddot{x}_E \sin\gamma) \tag{2-36}$$

Note $\dot{x}_E = v\cos\gamma$ and $\dot{z}_E = -v\sin\gamma$. Inserting the expressions for $\ddot{z}_E$ and $\ddot{x}_E$ yields

$$\begin{aligned}\dot{\gamma} = \frac{\bar{q}}{mv}\Big[&\left(L_0 + L_\alpha \alpha + L_{\delta_e}\delta_e\right) \\ &+ \left(D_0 + k_1\left(\alpha + \Delta_f \delta_f\right)^2 + k_2(\alpha + \Delta_e \delta_e)^2\right)\tan\alpha\Big] \\ &- \frac{g}{v}\left(\frac{\cos\theta}{\cos\alpha}\right)\end{aligned} \tag{2-37}$$

Drag is at generally a magnitude less than lift in most aircraft designs. Since the drag term is further reduced by $\tan\alpha$ in (2-37)—note the limits to α given in (2-33)—the following assumption is made to simplify the model.

Assumption 2.10 The drag term in (2-37) is insignificant relative to the lift term.

The drag term is dropped to yield

$$\dot{\gamma} \approx \frac{1}{mv}\left[\bar{q}\left(L_0 + L_\alpha \alpha + L_{\delta_e}\delta_e\right) - mg\left(\frac{\cos\theta}{\cos\alpha}\right)\right] \tag{2-38}$$

Incorporating the icing factors results in

$$\dot{\gamma} \approx \frac{1}{mv}\Big[\bar{q}\left[\sigma_{0_W}L_{0_W} + \sigma_{0_H}L_{0_H} + \left(\sigma_{\alpha_W}L_{\alpha_W} + \sigma_{\alpha_H}L_{\alpha_H}\right)\alpha + \sigma_{\delta_H}L_{\delta_e}\delta_e\right] - mg\left(\frac{\cos\theta}{\cos\alpha}\right)\Big] \tag{2-39}$$

With ϕ the vector of unknown parameters, the plant will be written in the form

$$\dot{x} = f(x,u) + g(x,u)\phi \tag{2-40}$$

Using the shorthand notation c_{x_3} for $\cos x_3$, $f(x,u)$, $g(x,u)$, and ϕ are

$$f(x,u) = \begin{bmatrix} x_2 \\ \bar{q}(M_0 + M_\alpha x_3) \\ x_2 + \frac{g}{v}\left(\frac{\cos(x_1+\bar{\theta})}{\cos x_3}\right) \end{bmatrix} \tag{2-41}$$

$$g(x,u) = \bar{q}\begin{bmatrix} 0 & 0 & 0 & 0 & 0 \\ M_{c0_W}c_{x_3} & M_{c0_H}c_{x_3} & M_{c\alpha_W}c_{x_3}x_3 & M_{c\alpha_H}c_{x_3}x_3 & M_{\delta_e}c_{x_3}u \\ -\frac{L_{0_W}}{mv} & -\frac{L_{0_H}}{mv} & -\frac{L_{\alpha_W}}{mv}x_3 & -\frac{L_{\alpha_H}}{mv}x_3 & -\frac{L_{\delta_e}}{mv}u \end{bmatrix} \tag{2-42}$$

$$\phi = \begin{bmatrix} \sigma_{0_W} \\ \sigma_{0_H} \\ \sigma_{\alpha_W} \\ \sigma_{\alpha_H} \\ \sigma_{\delta_H} \end{bmatrix} \qquad \phi \in \Phi = \begin{bmatrix} (0,1] \\ (0,1] \\ (0,1] \\ (0,1] \\ (0,1] \end{bmatrix} \tag{2-43}$$

Chapter 3

Design of a CEC

3.1 Overview

The CEC is obtained utilizing a recursive design procedure, known as backstepping, to derive a Lyapunov-based, feedback controller. The x_1-x_2 subsystem is stabilized via backstepping, with x_2 acting as the virtual control for x_1. A positive-definite Lyapunov-function with a negative-definite time-derivative will be used to show the stability of the closed-loop x_1-x_2 subsystem. The third state's differential equation will be considered a zero-dynamics subsystem, and will be shown to be stable with $x_1 = x_2 = 0$. Design of the controller will follow the process outlined in [17] for nonlinear block backstepping. All results presented hold for all $\phi \in \Phi$.

The plant (2-40) is rewritten in the following form, with $x = x_1$ and $\xi = [x_2 \quad x_3]^T$.

$$\begin{aligned} \dot{x} &= f(x) + g(x)y \\ \dot{\xi} &= m(x,\xi) + \beta(x,\xi)u \end{aligned} \tag{3-1}$$

where $y = h(\xi) = x_2$ acts as a virtual output for the ξ system. Associating (2-41), (2-42), and (2-43) with (3-1) yields

$$f(x) = f(x_1) = 0 \tag{3-2}$$

$$g(x) = g(x_1) = 1 \tag{3-3}$$

$$m(x,\xi) = m(x_1, x_2, x_3) = \begin{bmatrix} \bar{q}\left(M_0 + M_\alpha x_3 + \begin{bmatrix} M_{c0_W} \\ M_{c0_H} \\ M_{c\alpha_W} x_3 \\ M_{c\alpha_H} x_3 \end{bmatrix}^T \begin{bmatrix} \sigma_{0_W} \\ \sigma_{0_H} \\ \sigma_{\alpha_W} \\ \sigma_{\alpha_H} \end{bmatrix} \cos x_3 \right) \\ x_2 + \frac{g}{v}\left(\frac{\cos(x_1 + \bar{\theta})}{\cos x_3} \right) - \frac{\bar{q}}{mv} \begin{bmatrix} L_{0_W} \\ L_{0_H} \\ L_{\alpha_W} x_3 \\ L_{\alpha_H} x_3 \end{bmatrix}^T \begin{bmatrix} \sigma_{0_W} \\ \sigma_{0_H} \\ \sigma_{\alpha_W} \\ \sigma_{\alpha_H} \end{bmatrix} \end{bmatrix} \tag{3-4}$$

$$\beta(x,\xi) = \beta(x_1, x_2, x_3) = \begin{bmatrix} \bar{q} M_{\delta_e} \cos x_3 \, \sigma_{\delta_H} \\ -\frac{\bar{q} L_{\delta_e}}{mv} \sigma_{\delta_H} \end{bmatrix} \tag{3-5}$$

To apply nonlinear block backstepping, the following two conditions be met.

- The ξ subsystem must have a constant, globally-defined, relative degree of one uniformly in x.
- The zero dynamics subsystem of $\dot{\xi}$ must be Input-to-State Stable (ISS) with respect to $x = x_1$ and $y = x_2$ as inputs.

The conditions will be verified in Section 3.2 and Section 3.3.

3.2 Control Design for the Pitch Subsystem

The virtual control, x_2, will be such that the x_1 subsystem is stabilized when x_2 equals a desired $\alpha(x_1)$, with $V: \mathbb{R}^n \to \mathbb{R}$ a smooth, positive definite, radially unbounded function such that

$$\dot{V}(x_1) = \frac{\partial V}{\partial x_1}(x_1)[f(x_1) + g(x_1)\alpha(x_1)] \leq -W(x_1) < 0 \; \forall \; x_1 \backslash \{0\} \tag{3-6}$$

where $W: \mathbb{R}^n \to \mathbb{R}$ is positive definite.

To satisfy the first condition, $\frac{\partial y}{\partial \xi}(\xi)\beta(x,\xi) \neq 0$ for all $x \in \mathcal{X}$ and for all t_0:

$$\frac{\partial y}{\partial \xi}(\xi)\beta(x,\xi) = [1 \quad 0]\begin{bmatrix} \bar{q} M_{\delta_e} \cos x_3 \, \sigma_{\delta_H} \\ -\dfrac{\bar{q} L_{\delta_e}}{mv} \sigma_{\delta_H} \end{bmatrix} = \bar{q} M_{\delta_e} \cos x_3 \, \sigma_{\delta_H} \tag{3-7}$$

Noting that $\bar{q} \neq 0$, $M_{\delta_e} \neq 0$, and $\sigma_{\delta_H} \neq 0$, (3-7) is only zero when $x_3 = 90°$ or $x_3 = -90°$. The bounds on x_3, given in (2-33), are α_{s-} and α_{s+}, which are near the stall angle of attack. For a majority of aircraft, the limits on AOA (i.e., x_3) are within $\pm 20°$, and, given limits in aerodynamics, are never near $90°$; therefore, $\cos x_3 \neq 0$ for all x_3. With (3-7) non-zero for all $x \in \mathcal{X}$ and for all t_0, the relative degree is globally defined

and one uniformly in x. The nonlinearities in the input-output relationship (i.e., in $\dot{x}_2$) can be therefore cancelled with the input

$$u = \left(-c_1[y - \alpha(x)] - \frac{\partial h}{\partial \xi}(\xi) m(x,\xi) + \frac{\partial \alpha}{\partial x}(x)[f(x) + g(x)y] - \frac{\partial V}{\partial x}(x) g(x) \right) \left(\frac{\partial h}{\partial \xi}(\xi) \beta(x,\xi) \right)^{-1}, \tag{3-8}$$

which can also be written as

$$u = \left[-c_1[x_2 - \alpha(x)] - \bar{q} \left(M_0 + M_\alpha x_3 + \begin{bmatrix} M_{c0_W} \\ M_{c0_H} \\ M_{c\alpha_W} x_3 \\ M_{c\alpha_H} x_3 \end{bmatrix}^T \begin{bmatrix} \sigma_{0_W} \\ \sigma_{0_H} \\ \sigma_{\alpha_W} \\ \sigma_{\alpha_H} \end{bmatrix} \cos x_3 \right) + \frac{\partial \alpha}{\partial x}(x) x_2 - \frac{\partial V}{\partial x}(x) \right] \left(\bar{q} M_{\delta_e} \cos x_3 \, \sigma_{\delta_H} \right)^{-1} \tag{3-9}$$

where c_1 is a positive controller gain.

The virtual control, $\alpha(x_1)$, must be obtained such that x_1 is stabilized if $x_2 = \alpha(x_1)$. The following virtual control and Lyapunov function are chosen:

$$V(x_1) = \frac{1}{2} x_1^2 \tag{3-10}$$

$$\alpha(x_1) = -x_1 \tag{3-11}$$

The resulting $\dot{V}(x_1)$ is negative definite:

$$\dot{V}(x_1) = x_1 x_2 = -x_1^2 < 0 \; \forall \; x_1 \backslash \{0\} \tag{3-12}$$

Note (3-6) is now satisfied with $W(x) = kx_1^2$, where $0 < k \leq 1$. Controller (3-9) is now rewritten as

$$u = -\left[\bar{q}\left(M_0 + M_\alpha x_3 + \begin{bmatrix} M_{c0_W} \\ M_{c0_H} \\ M_{c\alpha_W} x_3 \\ M_{c\alpha_H} x_3 \end{bmatrix}^T \begin{bmatrix} \sigma_{0_W} \\ \sigma_{0_H} \\ \sigma_{\alpha_W} \\ \sigma_{\alpha_H} \end{bmatrix} \cos x_3\right) + (c_1 + 1)(x_1 + x_2)\right]\left(\bar{q} M_{\delta_e} \cos x_3 \, \sigma_{\delta_H}\right)^{-1} \tag{3-13}$$

Given the bounds on x_1, x_2, and x_3 given in (2-33)—particularly the bound on x_3 that ensures $\cos x_3 \neq 0 \; \forall \; x_3$—the input in (3-13) is bounded.

Substituting (3-13) in for the input in the system dynamics shown in (2-7) gives the following state differential-equations for x_1 and x_2:

$$\begin{bmatrix} \dot{x}_1 \\ \dot{x}_2 \end{bmatrix} = \begin{bmatrix} x_2 \\ -(c_1 + 1)(x_1 + x_2) \end{bmatrix} \tag{3-14}$$

Stability of (3-14) is shown via the positive definiteness of the Lyapunov function

$$V_1(x_1, x_2) = \frac{1}{2}[x_1^2 + (x_1 + x_2)^2] \tag{3-15}$$

and the negative definiteness of the time derivative

$$\dot{V}_1(x_1, x_2) = -[x_1^2 + c_1(x_1^2 + 2x_1x_2 + x_2^2)] \tag{3-16}$$

With $V_1(x_1, x_2)$ positive definite and $\dot{V}_1(x_1, x_2)$ negative definite, the control u stabilizes the x_1-x_2 subsystem.

3.3 AOA Subsystem and Analysis of the Zero Dynamics

Stability of the AOA—x_3—subsystem is now assessed as a zero-dynamics subsystem. To obtain the internal dynamics, the state, $\eta = \psi(x)$ is introduced such that

$$\mathcal{L}_\beta \psi(x) = 0 \tag{3-17}$$

(3-17) is satisfied with

$$\eta = \psi(x) = \overbrace{\frac{1}{M_{\delta_e}\sigma_{\delta_H}}}^{a_1} x_2 + \overbrace{\frac{mv}{L_{\delta_e}\sigma_{\delta_H}}}^{a_2} \sin x_3 = a_1 x_2 + a_2 \sin x_3 \tag{3-18}$$

where $a_1 < 0$, $a_2 > 0$, and, given the bounds on x_2 and x_3 in (2-33),

$$\eta \in \mathrm{H} = \left[a_1\dot{\theta}_+ + a_2 \sin \alpha_{s-}, a_1\dot{\theta}_- + a_2 \sin \alpha_{s+}\right] \subset \mathbb{R} \tag{3-19}$$

The internal dynamics, using the shorthand notation c_{x_3} for $\cos x_3$, is

$$\dot{\eta} = \mathcal{L}_m \psi(x) = \frac{1}{\sigma_{\delta_H}} \Bigg[\left(\frac{180}{\pi}\right) \frac{\bar{q}}{M_{\delta_e}} \left(M_0 + M_\alpha x_3 + \begin{bmatrix} M_{c0_W} \\ M_{c0_H} \\ M_{c\alpha_W} x_3 \\ M_{c\alpha_H} x_3 \end{bmatrix}^T \begin{bmatrix} \sigma_{0_W} \\ \sigma_{0_H} \\ \sigma_{\alpha_W} \\ \sigma_{\alpha_H} \end{bmatrix} c_{x_3} \right)$$

$$+ \frac{mv}{L_{\delta_e}} c_{x_3} \Bigg(x_2 + \left(\frac{180}{\pi}\right) \frac{g}{v} \left(\frac{\cos(x_1 + \bar{\theta})}{c_{x_3}} \right) \tag{3-20}$$

$$- \left(\frac{180}{\pi}\right) \frac{\bar{q}}{mv} \begin{bmatrix} L_{0_W} \\ L_{0_H} \\ L_{\alpha_W} x_3 \\ L_{\alpha_H} x_3 \end{bmatrix}^T \begin{bmatrix} \sigma_{0_W} \\ \sigma_{0_H} \\ \sigma_{\alpha_W} \\ \sigma_{\alpha_H} \end{bmatrix} \Bigg) \Bigg]$$

which is rewritten as

$$\dot{\eta} = b_0 + b_1 \cos(x_1 + \bar{\theta}) + (b_2 + b_3 x_2) \cos x_3 + (b_4 + b_5 \cos x_3) x_3 \tag{3-21}$$

where

$$b_0 = \left(\frac{180}{\pi}\right) \frac{\bar{q} M_0}{M_{\delta_e} \sigma_{\delta_H}} \qquad b_1 = \left(\frac{180}{\pi}\right) \frac{mg}{L_{\delta_e} \sigma_{\delta_H}}$$

$$b_2 = \left(\frac{180}{\pi}\right) \frac{\bar{q}}{\sigma_{\delta_H}} \left(\frac{1}{M_{\delta_e}} \begin{bmatrix} M_{c0_W} \\ M_{c0_H} \end{bmatrix}^T - \frac{1}{L_{\delta_e}} \begin{bmatrix} L_{0_W} \\ L_{0_H} \end{bmatrix}^T \right) \begin{bmatrix} \sigma_{0_W} \\ \sigma_{0_H} \end{bmatrix}$$

$$b_3 = \frac{mv}{L_{\delta_e} \sigma_{\delta_H}} \qquad b_4 = \left(\frac{180}{\pi}\right) \frac{\bar{q} M_\alpha}{M_{\delta_e} \sigma_{\delta_H}} \tag{3-22}$$

$$b_5 = \left(\frac{180}{\pi}\right) \frac{\bar{q}}{\sigma_{\delta_H}} \left(\frac{1}{M_{\delta_e}} \begin{bmatrix} M_{c\alpha_W} \\ M_{c\alpha_H} \end{bmatrix}^T - \frac{1}{L_{\delta_e}} \begin{bmatrix} L_{\alpha_W} \\ L_{\alpha_H} \end{bmatrix}^T \right) \begin{bmatrix} \sigma_{\alpha_W} \\ \sigma_{\alpha_H} \end{bmatrix}$$

With the controller bringing the states x_1 and x_2 to zero, the resulting zero dynamics is

$$\dot{\eta}_0 = b_0 + b_1 \cos\bar{\theta} + b_2 \cos x_3 + (b_4 + b_5 \cos x_3)x_3 \tag{3-23}$$

or, in terms of η_0,

$$\begin{aligned}\dot{\eta}_0 = b_0 + b_1 \cos\bar{\theta} + b_2 \cos\left[\sin^{-1}\left(\frac{\eta_0}{a_2}\right)\right] \\ + \left(b_4 + b_5 \cos\left[\sin^{-1}\left(\frac{\eta_0}{a_2}\right)\right]\right)\left(\frac{180}{\pi}\right)\sin^{-1}\left(\frac{\eta_0}{a_2}\right)\end{aligned} \tag{3-24}$$

Assessment of the stability of the zero dynamics necessitates an understanding of the magnitudes and signs of the b constants in (3-23) and (3-24). Keeping in mind Assumption 2.2:

- b_0 is positive if the fuselage contributes a positive moment at a zero AOA, negative if the moment is negative, or zero otherwise. Given Assumption 2.2, b_0 is small in magnitude.
- $b_1 \cos(x_1 + \bar{\theta})$ is large and positive for pitches near 0°. Note $x_1 + \bar{\theta}$ equals θ, the pitch angle. $\cos\theta$ can significantly reduce b_1 or change its sign. b_1 is proportional to the aircraft weight.
- b_2 is large and driven by the $-1/L_{\delta_e}\begin{bmatrix}L_{0_W} \\ L_{0_H}\end{bmatrix}^T$ term, which is negative and resembles the zero-AOA lift, which is generally close to the aircraft weight.
- b_3 is large and positive. b_3 is proportional to the aircraft's momentum.
- b_4 is positive if the fuselage contributes a stabilizing moment force (i.e., M_α is negative), negative if the fuselage contributes a destabilizing moment force (i.e.,

M_α is positive), and zero otherwise. Without a lifting fuselage (per Assumption 2.2), b_4, as with b_0, is significantly smaller than b_1 and b_2 in magnitude.

- b_5 is smaller than b_1 and b_2, but larger than b_0 and b_4. b_5 is driven by the $-1/L_{\delta_e}\begin{bmatrix}L_{\alpha_W}\\ L_{\alpha_H}\end{bmatrix}^T$ term, which is negative and resembles the change in lift per change in AOA. b_5 is, at most, a magnitude less than b_1 and b_2.

(3-23) equals zero at x_3^*, the point of equilibrium for $\dot{\eta}_0$, on which bounds can now be obtained. The bounds are

$$-\frac{b_0 - b_1 + b_2\cos\alpha_s}{b_4 + b_5\cos\alpha_s} \leq x_3^* \leq -\frac{b_0 + b_1 + b_2\cos\alpha_s}{b_4 + b_5\cos\alpha_s} \tag{3-25}$$

The value of x_3^* is mainly impacted by $\bar{\theta}$, which impacts the magnitude and sign of b_1 in the numerator. The resulting point of equilibrium in the zero dynamics is

$$\eta_0^* = a_2 \sin x_3^* \tag{3-26}$$

The zero dynamics (3-24) is now linearized at the equilibrium point $[x_1^* \quad x_2^* \quad \eta_0^*]^T$. Noting the derivatives

$$\frac{\partial\left(\sin^{-1}\left(\frac{\eta_0}{a_2}\right)\right)}{\partial\eta_0} = \left(\frac{180}{\pi}\right)\frac{1}{\sqrt{a_2^2 - \eta_0^2}} \tag{3-27}$$

$$\frac{\partial\left(\cos\left[\sin^{-1}\left(\frac{\eta_0}{a_2}\right)\right]\right)}{\partial\eta_0} = -\left(\frac{180}{\pi}\right)\frac{\eta_0}{a_2\sqrt{a_2^2 - \eta_0^2}} \tag{3-28}$$

and

$$\cos\left[\sin^{-1}\left(\frac{\eta_0}{a_2}\right)\right] = \frac{\sqrt{a_2^2 - \eta_0^2}}{a_2} \tag{3-29}$$

the partial derivative of (3-24) with respect to $[x_1 \quad x_2 \quad \eta_0]^T$ (evaluated at $[x_1^* \quad x_2^* \quad \eta_0^*]^T$) is

$$A_\eta = \left(\frac{180}{\pi}\right)\left(\frac{b_4 - \frac{\eta_0^*}{a_2}\left[b_2 + \left(\frac{180}{\pi}\right) b_5 \sin^{-1}\left(\frac{\eta_0^*}{a_2}\right)\right]}{\sqrt{a_2^2 - {\eta_0^*}^2}} + \frac{b_5}{a_2}\right) \tag{3-30}$$

Where the linearized zero dynamics is

$$\dot{\eta}_0 = A_\eta(\eta_0 - \eta_0^*) \tag{3-31}$$

Local stability of the zero dynamics can now be assessed by evaluating the sign of A_η—if $A_\eta < 0$ at the equilibrium η_0^*, the zero dynamics is locally exponentially stable. Although the case for most aircraft, there is no absolute guarantee that η_0^* satisfies the condition $A_\eta < 0$, thus warranting the following assumption.

Assumption 3.1 The equilibrium η_0^* of the zero dynamics (3-24) satisfies

$$\frac{b_4 - \frac{\eta_0^*}{a_2}\left[b_2 + \left(\frac{180}{\pi}\right) b_5 \sin^{-1}\left(\frac{\eta_0^*}{a_2}\right)\right]}{\sqrt{a_2^2 - {\eta_0^*}^2}} + \frac{b_5}{a_2} < 0 \tag{3-32}$$

For aircraft abiding by Assumption 2.2, (3-32) is negative in between the two roots—the values of η_0^* where (3-32) equals zero.

Given Assumption 3.1, A_η is negative at the equilibrium point η_0^*, and the system, therefore, is locally exponentially stable and ISS, thus satisfying the second condition for nonlinear block backstepping given in Section 3.1. With both conditions met, the input (3-13) will make the system asymptotically stable.

Chapter 4

Implementation of the BaLSI

The BaLSI considers systems of the form (with $k: \Phi \times \mathcal{X} \to \mathcal{U}$)

$$\begin{aligned} & \dot{x} = f(x,u) + g(x,u)\phi \\ x \in \mathcal{X} \subset \mathbb{R}^n \qquad & u = k(\phi,x) \in \mathcal{U} \subset \mathbb{R}^m \qquad \phi \in \Phi \subset \mathbb{R}^l \end{aligned} \tag{4-1}$$

The aircraft plant was organized as such in Section 2.4, with, respectively, $f(x,u)$, $g(x,u)$, and ϕ given in (2-41), (2-42), and (2-43), $\mathcal{X}$, $\mathcal{U}$, and Φ given in (2-33), (2-34), and (2-43), and $n = 3$, $m = 1$, and $l = 5$.

Implementation of the BaLSI is preceded by the following two assumptions, with $\rho > 0$ and $V(\phi,x)$ a family of continuously-differentiable, positive-definite, radially-unbounded functions.

Assumption 4.1 The inequality

$$\nabla V(\phi,x)\left[f\left(x,k(\phi,x)\right) + g\left(x,k(\phi,x)\right)\phi\right] \leq -2\rho V(\phi,x) \tag{4-2}$$

with $\rho > 0$ holds for the closed-loop system (4-1) for all $\phi \in \Phi$ and $x \in \mathcal{X}$.

Assumption 4.2 For every $\bar{\Phi} \subseteq \Phi$, for every $M \geq 0$, there exists $R > 0$ such that, given $V(\phi,x) \leq M$, $|x| \leq R$ for all $\phi \in \bar{\Phi}$.

The BaLSI methodology employs an event-triggered approach to update the parameter estimate, $\hat{\phi}$, as opposed to a continuous update. In between event triggers, the parameter estimate is held constant, as described below:

$$\begin{matrix} u(t) = k\left(\hat{\phi}(\tau_i), x(t)\right) \\ \hat{\phi}(t) = \hat{\phi}(\tau_i) \end{matrix} \qquad t \in [\tau_i, \tau_{i+1}) \tag{4-3}$$

where $i \in \mathbb{Z}_{\geq 0}$, and τ_i is the time of the ith event-trigger:

$$\begin{matrix} \tau_i \geq 0 \qquad \tau_0 = 0 \\ \tau_{i+1} = \min\{\tau_i + T, r_i\} \end{matrix} \tag{4-4}$$

T is the maximum allotted time before a parameter update is forced, and $r_i > \tau_i$ is the time of the trigger, where r_i is the lowest $t > \tau_i$ at which

$$V\left(\hat{\phi}(\tau_i), x(t)\right) = V\left(\hat{\phi}(\tau_i), x(\tau_i)\right) + a\big(x(\tau_i)\big) + \epsilon \tag{4-5}$$

where $a: \mathbb{R}^n \to \mathbb{R}_{\geq 0}$ is a continuous, positive-definite function and $\epsilon > 0$ is constant. With the trigger mechanism derived, the BaLSI will now be derived.

Given (4-1), with $t, s \geq t_0$, variation of constants gives

$$x(t) - x(s) = \int_s^t f\big(x(r), u(r)\big)dr + \left(\int_s^t g\big(x(r), u(r)\big)dr\right)\phi \tag{4-6}$$

The function $h_i: \mathbb{R}^l \to \mathbb{R}_+$, for every $i \in \mathbb{Z}_{\geq 0}$, is defined as

$$h_i(\varphi) \coloneqq \int_{t_0}^{\tau_{i+1}} \int_{t_0}^{\tau_{i+1}} |p(t,s) - q(t,s)\varphi|^2 ds\, dt \tag{4-7}$$

given

$$p(t,s) \coloneqq x(t) - x(s) - \int_s^t f\big(x(r), u(r)\big) dr \tag{4-8}$$

$$q(t,s) \coloneqq \int_s^t g\big(x(r), u(r)\big) dr \tag{4-9}$$

$h_i(\varphi)$ has a global minimum at $\varphi = \phi$, where $h_i(\phi) = 0$. Noting $q^T(t,s)p(t,s) = q^T(t,s)q(t,s)\phi$, the following holds:

$$Z(\tau_{i+1}) = G(\tau_{i+1})\phi \tag{4-10}$$

where

$$Z(\tau_i) = \int_{t_0}^{\tau_{i+1}} \int_{t_0}^{\tau_{i+1}} q^T(t,s)p(t,s) ds\, dt \tag{4-11}$$

$$G(\tau_i) = \int_{t_0}^{\tau_{i+1}} \int_{t_0}^{\tau_{i+1}} q^T(t,s)q(t,s) ds\, dt \tag{4-12}$$

$G(\tau_i)$ is positive semidefinite, and, therefore, if the determinant of $G(\tau_i)$ is nonzero, the vector of unknown parameters can be calculated as

$$\phi = \left(G(\tau_{i+1})\right)^{-1} Z(\tau_{i+1}) \tag{4-13}$$

which is a least-squares estimate of ϕ. The convex optimization problem

$$\begin{aligned} &\min_{\varphi \in \Phi} \left|\varphi - \hat{\phi}(\tau_i)\right| \\ &s.t. \quad Z(\tau_{i+1}) = G(\tau_{i+1})\varphi \end{aligned} \tag{4-14}$$

results in the parameter update law

$$\hat{\phi}(\tau_{i+1}) = \text{argmin}\left\{\left|\varphi - \hat{\phi}(\tau_i)\right|^2 : \varphi \in \Phi, Z(\tau_{i+1}) = G(\tau_{i+1})\varphi\right\} \tag{4-15}$$

The parameter update law (4-15) is the BaLSI, which is to be utilized at the event triggers as described in (4-4).

$G(\tau_i)$, however, is not necessarily invertible due to possible measurement and modeling errors in the plant. Although (4-10) holds when no errors are present, there is no guarantee that the set of $\varphi \in \Phi$, such that (4-10) holds, is nonempty. Therefore, the minimization problem is relaxed to yield

$$\hat{\phi}(\tau_{i+1}) = \text{argmin}\left\{\left|\varphi - \hat{\phi}(\tau_i)\right|^2 + \beta |Z(\tau_{i+1}) - G(\tau_{i+1})\varphi|^2 : \varphi \in \Phi\right\} \tag{4-16}$$

where $\beta > 0$ is a large constant, and

$$\hat{\phi}(\tau_{i+1}) = \left(\beta^{-1} I + G^2(\tau_{i+1})\right)^{-1} \left(\beta^{-1}\hat{\phi}(\tau_i) + G(\tau_{i+1}) Z(\tau_{i+1})\right) \tag{4-17}$$

With (4-16), in the case where $\Phi = \mathbb{R}^l$, with $G^2(\tau_{i+1})$ positive semidefinite and $\beta^{-1}I$ positive definite, the resulting $\beta^{-1}I + G^2(\tau_{i+1})$ is positive definite and, therefore, invertible.

The BaLSI can be implemented by the following set of Ordinary Differential Equations (ODEs)

$$z \in \mathbb{R}^j \qquad \dot{z} = \bar{C}x \tag{4-18}$$

$$B \in \mathbb{R}^{l \times j} \qquad \dot{B} = t\big(\bar{C}g(x,u)\big)^T \tag{4-19}$$

$$w \in \mathbb{R}^l \qquad \dot{w} = \big(\bar{C}g(x,u)\big)^T(z+\gamma) + B\bar{C}f(x,u) \tag{4-20}$$

$$\gamma \in \mathbb{R}^j \qquad \dot{\gamma} = t\bar{C}f(x,u) \tag{4-21}$$

$$Y \in \mathbb{R}^l \qquad \dot{Y} = 2(B\bar{C}x - w) \tag{4-22}$$

$$Q \in \mathbb{R}^{l \times l} \qquad \ddot{Q} = 2\big(B\bar{C}g(x,u)\big)^T + 2B\bar{C}g(x,u) \tag{4-23}$$

with the initial conditions

$$\begin{gathered} z(0) = \gamma(0) = 0 \qquad Q(0) = \dot{Q}(0) = 0 \\ B(0) = 0 \qquad Y(0) = w(0) = 0 \end{gathered} \tag{4-24}$$

and the parameter update law

$$\hat{\phi}(\tau_{i+1}) = \operatorname{argmin}\left\{\left|\varphi - \hat{\phi}(\tau_i)\right|^2 + \beta|Y(\tau_{i+1}) - Q(\tau_{i+1})\varphi|^2 : \varphi \in \Phi\right\} \tag{4-25}$$

where $\bar{C}$ is a selection matrix utilized when the parameter ϕ appears in $j < n$ equations of the $\dot{x}$ equations. If ϕ appears in $\dot{x}_{k_1}, \cdots, \dot{x}_{k_j}$, where $k_1, \cdots, k_j \in \{1, \cdots, n\}$, then $\bar{C} \in \mathbb{R}^{j \times n}$ is such that $\bar{c}_{1,k_1} = \bar{c}_{2,k_2} = \cdots = \bar{c}_{j,k_j} = 1$ ($\bar{c}_{r,s} = 0$ otherwise)—note that if $j = n$, then $\bar{C} \in \mathbb{R}^{n \times n}$ would be an identity matrix. With the impact of the unknown parameter vector, ϕ, limited to $\dot{x}_2$ and $\dot{x}_3$, as seen in (2-42), the resulting $\bar{C}$ for the aircraft plant is

$$\bar{C} = \begin{bmatrix} 0 & 1 & 0 \\ 0 & 0 & 1 \end{bmatrix} \tag{4-26}$$

In summary, there are four tunable parameters for the BaLSI:

- $T > 0$, a constant, is the maximum time allowed without a parameter update.
- $a(x)$, a continuous, positive-definite function, is used for the event trigger.
- $\epsilon > 0$, a constant, is utilized for practical implementation of the trigger to avoid a constant trigger at $x(\tau_i) = 0$.
- $\beta > 0$, a large constant, is utilized to aid in the solving of the optimization problem presented in (4-14).

[15] gives encouraging results on the stability of the BaLSI, given compliance to the assumptions presented. For the aircraft system, the assumptions only hold for the x_1-x_2

subsystem and not the zero dynamics (i.e., the x_3 subsystem). Given V_1 in (3-15) and $\dot{V}_1$ in (3-16) (recall c_1 is a positive constant), (4-2) can be rewritten for the system as

$$x_1^2 + c_1(x_1 + x_2)^2 \geq \rho[x_1^2 + (x_1 + x_2)^2] \tag{4-27}$$

Inequality (4-3), and, therefore, Assumption 4.1, can be satisfied for the x_1-x_2 subsystem for any positive ρ if

$$\rho \leq \min\{1, c_1\} \tag{4-28}$$

Young's Inequality is applied to (3-15) to obtain

$$V_1(x_1, x_2) = \frac{1}{2}[x_1^2 + (x_1 + x_2)^2] \leq \frac{3}{2}(x_1^2 + x_2^2) \tag{4-29}$$

Assumption 4.2, therefore, is satisfied for the x_1-x_2 subsystem with

$$R = \sqrt{\frac{2}{3}M} \tag{4-30}$$

With the exclusion of the zero dynamics subsystem, guarantees made by [15] on the solution will be restricted.

For the purpose of spelling out clearly the guarantees provided by the design developed in this work, the following theorem is provided, as a direct extension from Theorem 4.1 in [15], and applied to the aircraft plant derived in Section 2.4, the controller derived in Chapter 3, and the BaLSI scheme given by (4-3), (4-4), (4-5), (4-16), and (4-18) through (4-24). The aircraft plant is given in (2-40), with,

respectively, $f(x,u)$, $g(x,u)$, and ϕ given in (2-41), (2-42), and (2-43) and the states and input defined in (2-33) and (2-34), respectively. The shorthand notation $x^{(i)}$ refers to the ith state.

Theorem 4-1 Consider the aircraft plant given in (2-40) with the input (3-13), the parameter update law (4-25), and initial conditions $x(t_0) = x_0 \in \mathcal{X}$ and $\hat{\phi}(t_0) = \hat{\phi}_0 \in \Phi$. Let the x_1-x_2 subsystem be subject to Assumption 4.1 and Assumption 4.2, and the zero-dynamics subsystem be subject to Assumption 3.1. Let $T > 0$ be a constant and let $a: \mathbb{R}^n \to \mathbb{R}_+$ be a continuous, positive-definite function. Then, there exists a family of class $\mathcal{KL}$ mappings $\omega_{\phi,\hat{\phi}}$, parametrized by $\phi, \hat{\phi} \in \Phi$, such that for every $\phi \in \Phi$, $x_0 \in \mathcal{X}$, and $\hat{\phi}_0 \in \Phi$, the solution of the closed-loop system is unique, is defined for all $t \geq t_0$, and satisfies

$$|x(t-t_0)| \leq \omega_{\phi,\hat{\phi}_0}(|x_0|, t-t_0) \tag{4-31}$$

Moreover, there exists a $\tau \geq 0$ and $\phi_s \in \Phi$ (both depending on ϕ, t_0, and the initial conditions) such that $\hat{\phi}(t) = \phi_s$ for all $t \geq t_0 + \tau$ and $g\big(t, x(t), u(t)\big)(\phi - \phi_s) = 0$ for all $t \geq t_0$. Furthermore, the estimate $\hat{\phi}_i$ at $\tau_i \geq (i-l)T$ holds for all $i \geq l$.

Theorem 4-1 guarantees—without requirement for persistency of excitation—convergence of the parameter estimate and the existence of a finite settling time for the estimate; however, there is no upper bound on the settling time. [15] further guarantees, in Theorem 4.2, local and global exponential stabilization of the closed-loop system

with BaLSI implementation as long as the nominal feedback law achieves such. Proofs are provided for both theorems in [15].

Chapter 5

Simulation of an Aircraft in Icing

The control scheme presented is now applied to a Lockheed Martin C-5 Galaxy, a large military transport aircraft utilized by the United States Air Force (USAF). The C-5 Galaxy has been examined in various disciplines for performance optimization, such as formation-flight optimization utilizing extremum-seeking feedback control [18]. The model derived in Chapter 2 requires knowledge of various aircraft parameters. Mass, inertial, and a portion of the aerodynamic parameters are provided in [19], with remaining aerodynamic information estimated utilizing three-view drawings of the aircraft and approximated airfoil data. Using methods presented in [20] and [21], the acquired data is then utilized to estimate the various parameters required for the model.

For the model, the mass, m, employed is that of the aircraft with about half of the maximum fuel capacity—$1.76(10)^4\ slugs$. The air density and gravity (g) used—32.1 $ft/_{s^2}$ and $1.07(10)^{-3}\ slugs/_{ft^3}$—are the values at 25,000 ft above sea level.

The airspeed, v, is set to 700 $^{ft}/_{S}$. The lift, drag, and moment parameters in (2-7), (2-12), and (2-27) are evaluated for the aircraft in the following equations:

$$\begin{gathered} L_{0_W} = 2.19(10)^3\, ft^2 \quad L_{0_H} = -75.8\, ft^2 \\ L_{\alpha_W} = 447\frac{ft^2}{1^\circ} \qquad L_{\alpha_H} = 53.0\frac{ft^2}{1^\circ} \qquad L_{\delta_e} = 15.9\frac{ft^2}{1^\circ} \end{gathered} \tag{5-1}$$

$$\begin{gathered} D_{0_A} = 43.6\, ft^2 \qquad D_{0_W} = 48.0\, ft^2 \qquad D_{0_H} = 1.47\, ft^2 \\ k_1 = 1.14(10)^{-2}\, ft^2 \qquad k_2 = 1.11(10)^{-3}\, ft^2 \end{gathered} \tag{5-2}$$

$$\begin{gathered} M_0 = 0\ \frac{ft}{slug} \qquad M_\alpha = -5.85(10)^{-5}\ \frac{ft}{slug\text{-}1^\circ} \\ M_{c0_W} = -1.03(10)^{-4}\ \frac{ft}{slug} \qquad M_{c0_H} = 3.52(10)^{-4}\ \frac{ft}{slug} \\ M_{c\alpha_W} = -2.11(10)^{-5}\ \frac{ft}{slug\text{-}1^\circ} \qquad M_{c\alpha_H} = -2.46(10)^{-4}\ \frac{ft}{slug\text{-}1^\circ} \\ M_{\delta_e} = -7.39(10)^{-5}\ \frac{ft}{slug\text{-}1^\circ} \end{gathered} \tag{5-3}$$

The icing factors selected are

$$\begin{aligned} \phi &= [\sigma_{0_W} \quad \sigma_{0_H} \quad \sigma_{\alpha_W} \quad \sigma_{\alpha_H} \quad \sigma_{\delta_H}]^T \\ &= [0.850 \quad 0.985 \quad 0.820 \quad 0.982 \quad 0.979]^T \end{aligned} \tag{5-4}$$

Attention is now given to the assumption levied in the derivation of the controller. Assumption 3.1 assumed the equilibrium point of the zero dynamics in (3-24) is such that (3-32) is satisfied in order to ensure local stability. With equilibrium at $\eta_0^* = 1.25(10)^4$, (3-32)—and Assumption 3.1—is satisfied with $A_\eta = -22.0 < 0$.

Bounds on the states and input, given in (2-33) and (2-34), are evaluated for the aircraft to be

$$x \in \mathcal{X} = \begin{bmatrix} [0 - \bar{\theta}°, 180° - \bar{\theta}] \\ [-10\,°/s\,, 10\,°/s] \\ [-10°, 10°] \end{bmatrix} \qquad u \in \mathcal{U} = [-30°, 30°] \tag{5-5}$$

Using the shorthand notation c_{x_3} for $\cos x_3$, the plant presented in (2-40), (2-41), and (2-42) is evaluated for the aircraft as follows:

$$\dot{x} = f(x,u) + g(x,u)\phi \tag{5-6}$$

$$f(x,u) = \begin{bmatrix} x_2 \\ -0.875x_3 \\ x_2 + 2.63\left(\dfrac{\cos(x_1 + \bar{\theta})}{\cos x_3}\right) \end{bmatrix} \tag{5-7}$$

$$g(x,u) = -\begin{bmatrix} 0 & 0 & 0 & 0 & 0 \\ 1.55\mathrm{c}_{x_3} & -5.26\mathrm{c}_{x_3} & 0.316\mathrm{c}_{x_3}x_3 & 3.68\mathrm{c}_{x_3}x_3 & 1.11\mathrm{c}_{x_3}u \\ 2.66 & -0.0918 & 0.542x_3 & 0.0642x_3 & 0.0193u \end{bmatrix} \tag{5-8}$$

The feedback input (3-13), with the gain $c_1 = 1$, is evaluated to be

$$\begin{aligned} u = \big[-0.875x_3 - \big(1.55\hat{\sigma}_{0_W} - 5.26\hat{\sigma}_{0_H} + 0.316x_3\hat{\sigma}_{\alpha_W} + 3.68x_3\hat{\sigma}_{\alpha_H}\big)\mathrm{c}_{x_3} \\ + 2(x_1 + x_2)\big]\big(1.11\mathrm{c}_{x_3}\hat{\sigma}_{\delta_H}\big)^{-1} \end{aligned} \tag{5-9}$$

where $\hat{\sigma}$ is an estimate of σ. The BaLSI scheme utilized the following parameters:

$$T = 1 \qquad V(\phi, x) = \frac{1}{2}(x_1^2 + x_2^2 + x_3^2) \qquad a(x) = x_1^2 + x_2^2 + x_3^2$$
$$\epsilon = 0 \qquad \beta = 10^9 \tag{5-10}$$

The simulation marched the states through time utilizing the differential equations given in (5-6). However, the effects of Assumption 2.10, which simplified the equation for $\dot{x}_3$, were removed to provide a realistic simulation environment. The aircraft was commanded to a five-degree pitch (i.e., $\bar{\theta} = 5°$), with a pitch, pitch rate, and AOA of zero for the initial conditions.

Figure 5-1 and Figure 5-2 plot the states (pitch, pitch rate, and AOA) and parameter estimates, respectively, versus time.

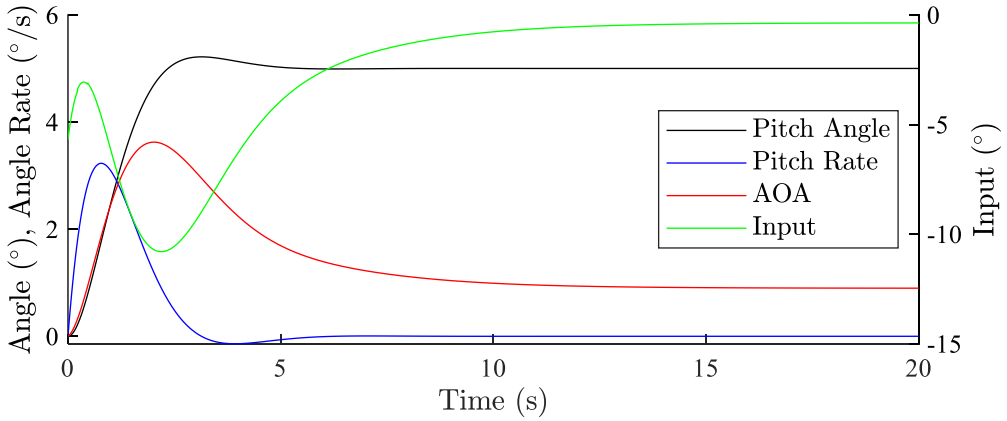

Figure 5-1 State History

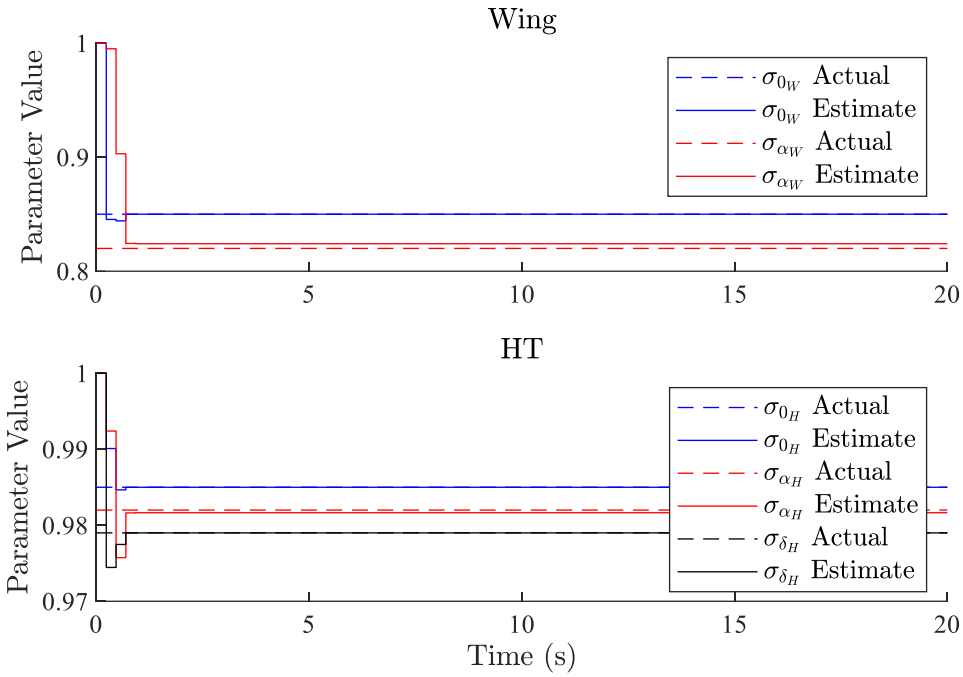

Figure 5-2 Parameter Estimates

Figure 5-1 showcases the effectiveness of the controller, with the commanded pitch reached with a steady-state error on the magnitude of 10^{-6}. Figure 5-2 shows the effectiveness of the BaLSI, with the parameter estimates converging to or near the actual values. The simulation was run without the simplification of Assumption 2.10. Thus, small errors in the parameter estimates, as in σ_{α_W} and σ_{α_H}, are expected due to Assumption 2.10 levied in the derivation of the plant.

A phase portrait for x_1-x_3 of the system response with the parameters known (the nominal case), the parameters unknown, and the parameters estimated with the BaLSI is given in Figure 5-3.

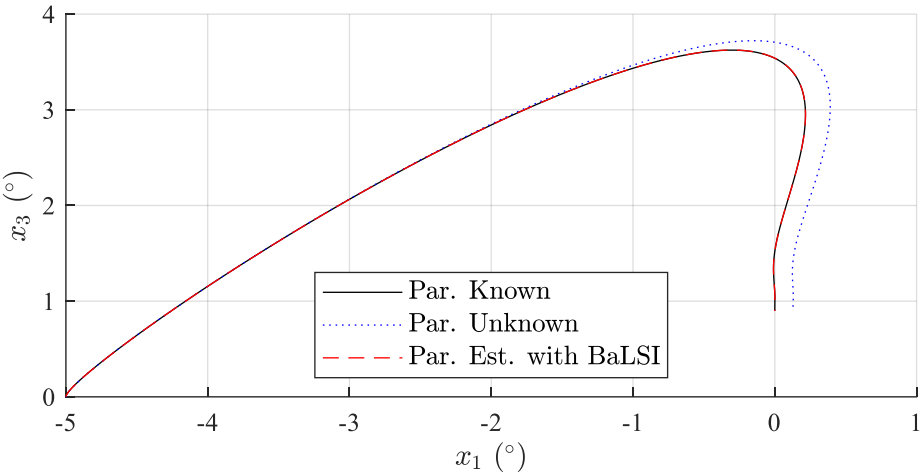

Figure 5-3 Phase Portrait

The nominal behavior seen in Figure 5-3 is closely followed by the system behavior with BaLSI implemented. With the parameters unknown, the system response deviates from nominal as expected, resulting in a noticeable steady-state error in pitch. With the BaLSI, the parameter-estimate convergence prevented any significant deviation from nominal behavior.

Chapter 6

Conclusions and Recommendations

6.1 Conclusions

An aircraft model was derived, with the impacts due to icing—specifically the decrease to lift and increase to drag—also modeled. A plant was constructed with the icing factors extracted into a single parameter vector, and a CEC derived via backstepping to stabilize the nominal system. The BaLSI was incorporated into the control scheme to estimate the five icing factors.

The control scheme was applied to the model of a Northrop Grumman C-5 Galaxy. The aircraft was simulated in icing with the parameters known, unknown, and estimated via the BaLSI. The BaLSI efficiently estimated the unknown parameters, as seen in Figure 5-2, allowing the system to closely follow the nominal behavior, as seen in Figure 5-3.

6.2 Recommendations

Although the accuracy of the BaLSI is sufficient for aircraft applications, subject to the assumptions presented, difficulties arise in the practical implementation of the scheme. According to [15], the BaLSI requires 46 first-order ODEs to be solved;

thus, the computational and memory requirements may exceed the capabilities of inexpensive flight computers. Furthermore, discrete-time application of the BaLSI requires a small timesteps in order to produce accurate estimations. Errors induced by the implementation in a discrete-time system can be expected to propagate over long periods of time. Since switching of the parameter-estimate values only need to occur l times, error propagation can be minimized by ensuring the trigger events cease before errors manifest.

Without any guarantee of an upper bound on the settling time of the parameter estimate, safe operation of the BaLSI would necessitate further work to ensure an acceptable settling time for application in aircraft. However, the short settling-time in the simulation is promising. Performance can be improved by tailoring the BaLSI parameters detailed in Chapter 4, particularly T. Reduction in T would reduce the settling time; however, T must maintain a safe distance from the timestep at which the aircraft's discrete-time system operates at.

Performance of the BaLSI is hampered by the presence of errors in measurements and modeling of the icing factors. Regarding the latter, icing is time varying, contrary to Assumption 2.9. Research into the time-varying behavior of icing, along with the BaLSI's handling of such behavior, would significantly improve the effectiveness of the identifier.

Lastly, accurate measurements of all states may not be available. AOA sensors can be inaccurate, especially for use in controllers, and, therefore, are typically

estimated utilizing a combination of inertial sensors and aerodynamic properties. While AOA readings are difficult to attain, pitch and pitch rate can be obtained utilizing an inertial navigation system, which may be influenced by noise. The performance of the BaLSI in the presence of noise must be assessed to ensure the BaLSI maintains effectiveness.

6.3 Acknowledgements

This thesis, in part, is currently being prepared for submission for publication of the material. Shaghoury, Samer; Krstić, Miroslav. The thesis author was the primary investigator and author of this material.

Chapter 7

Bibliography

[1] J. J. Reinmann, R. J. Shaw and R. J. Ranaudo, "NASA's Program on Icing Research and Technology," Cleveland, Ohio, USA, 1989.

[2] A. Heinrich, R. Ross, G. Zumwalt, J. Provorse, V. Padmanabhan, J. Thompson and J. Riley, "Aircraft Icing Handbook," Federal Aviation Administration, Wichita, Kansas, USA, 1991.

[3] Federal Aviation Administration, "Aviation Weather," Federal Aviation Administration, Washington, District of Columbia, USA, 2016.

[4] Federal Aviation Administration, "Pilot Guide: Flight in Icing Conditions," Federal Aviation Administration, Washington, District of Columbia, USA, 2015.

[5] R. W. Gent, N. P. Dart and J. T. Cansdale, "Aircraft Icing," *Philosophical Transactions: Mathematical, Physical and Engineering Sciences,* vol. 358, no. 1776, pp. 2873-2911, 15 November 2000.

[6] K. Szilder and E. P. Lozowski, "Novel Two-dimensional Modeling Approach for Aircraft Icing," *Journal of Aircraft,* vol. 41, no. 4, pp. 854-861, August 2004.

[7] T. P. Ratvasky, B. P. Barnhart and S. Lee, "Current Methods Modeling and Simulating Icing Effects on Aircraft Performance, Stability, Control," *Journal of Aircraft,* vol. 47, no. 1, pp. 201-211, February 2010.

[8] T. Lombaerts, S. Schuet, D. Acosta, J. Kaneshige, K. Shish and L. Martin, "Piloted Simulator Evaluation of Maneuvering Envelope Information for Flight Crew Awareness," *AIAA Guidance, Navigation, and Control Conference,* pp. 2448-2471, January 2015.

[9] A. Cristofaro, T. A. Johansen and A. P. Aguiar, "Icing Detection and Identification for Unmanned Aerial Vehicles Using Adaptive Nested Multiple

Models," *International Journal of Adaptive Control and Signal Processing,* vol. 31, no. 11, pp. 1584-1607, November 2017.

[10] N. Hovakimyan and C. Cao, $\mathscr{L}1$ Adaptive Control Theory, R. C. Smith, Ed., Philadelphia, Pennsylvania: Society for Industrial and Applied Mathematics, 2010, pp. 241-259.

[11] E. Xargay, N. Hovakimyan, V. Dobrokhodov, I. Kaminer, C. Cao and I. M. Gregory, "$\mathscr{L}1$ Adaptive Control in Flight," in *Advances in Intelligent and Autonomous Aerospace Systems*, vol. 241, J. Valasek, Ed., Reston, Virginia: American Institute of Aeronautics and Astronautics, 2012, pp. 129-172.

[12] C. Hou, L. Hu and Y. Zhang, "Adaptive Output Tracking Control for Nonlinear Systems with Failed Actuators and Aircraft Flight System Applications," *Mathematical Problems in Engineering,* May 2015.

[13] M. K. Rankin, "Adaptive Control of Aircraft in Uncertain Icing Conditions," Charlottesville, Virginia, USA, 2014.

[14] E. N. Hartley, "Predictive Control with Parameter Adaptation to Achieve α-Protection in the RECONFIGURE Benchmark in the Presence of Icing," *International Federation of Automatic Control,* vol. 48, no. 23, pp. 172-177, September 2015.

[15] I. Karafyllis, M. Kontorinaki and M. Krstić, "Adaptive Control By Regulation-Triggered Batch Least-Squares Estimation of Non-Observable Parameters," Cornell University Library, Ithaca, New York, USA, 2018.

[16] M. Bagheri, I. Karafyllis, P. Naseradinmousavi and M. Krstić, "Adaptive Control of a Two-Link Robot Using Batch Least-Square Identifier," 2020.

[17] M. Krstić, I. Kanellakopoulos and P. Kokotović, Nonlinear and Adaptive Control Design, S. Haykin, Ed., New York, NY: John Wiley & Sons, Inc., 1995.

[18] P. Binetti, K. B. Ariyur, M. Krstić and F. Bernelli, "Formation Flight Optimization Using Extremum Seeking Feedback," *Journal of Guidance, Control, and Dynamics,* vol. 26, no. 1, pp. 132-142, January-February 2003.

[19] T. R. Yechout, S. L. Morris, D. E. Bossert and W. F. Hallgren, Introduction to Aircraft Flight Mechanics, J. A. Schetz, Ed., Reston, Virginia: American Institute of Aeronautics and Astronautics, 2003.

[20] D. P. Raymer, Aircraft Design: A Conceptual Approach, 2nd ed., J. S. Przemieniecki, Ed., Washington, D.C.: American Institute of Aeronautics and Astronautics, 1992.

[21] Douglas Aircraft Company, Inc., USAF Stability and Control DATCOM, Wright-Patterson AFB, Ohio, 1965.